PHYSICAL REVIEW A **83**, 041803(R) (2011)

Observation of atomic localization using electromagnetically induced transparency

N. A. Proite, Z. J. Simmons, and D. D. Yavuz
Department of Physics, University of Wisconsin–Madison, 1150 University Avenue, Madison, Wisconsin 53706, USA
(Received 5 November 2010; published 22 April 2011)

We present a proof-of-principle experiment in which the population of an atomic level is spatially localized using the technique of electromagnetically induced transparency (EIT). The key idea is to utilize the sensitive dependence of the dark state of EIT on the intensity of the coupling laser beam. By using a sinusoidal intensity variation (standing wave), we demonstrate that the population of a specific hyperfine level can be localized much more tightly than the spatial period.

DOI: 10.1103/PhysRevA.83.041803 PACS number(s): 42.25.Kb, 32.80.Qk, 42.50.Gy

It is well known that traditional optical techniques cannot resolve or write features smaller than half the wavelength of light. This barrier, known as the diffraction limit, has important implications for a variety of scientific research areas, including biological microscopy and quantum computation. As an example, in a neutral-atom quantum computing architecture, the diffraction limit prohibits high-fidelity manipulation of individual atoms if they are separated by less than the wavelength of light. Recently, Agarwal and others [1–3] have proposed to use the dark state of electromagnetically induced transparency (EIT) [4,5] to address atoms at potentially nanometer spatial scales. This technique relies on the sensitive dependence of the dark state on the intensities of the driving probe and coupling laser beams. If a standing-wave coupling laser is used, the population of the excited Raman level can be very tightly localized near the intensity nodes, allowing for subwavelength control. In this letter, we present a proof-of-principle experiment that demonstrates the key ideas of this approach. By using ultracold rubidium (Rb) atoms in a magneto-optical trap (MOT) and pulsed coherent transfer, we demonstrate atomic localization to spots much smaller than the spatial period of the coupling-laser intensity profile. Although due to imaging limitations we have used a large spatial period in this work ($\sim 600\ \mu$m), our results will likely scale to the subwavelength regime in the future.

Before proceeding, we cite important prior work leading up to this experiment. In their pioneering work, Thomas and colleagues have suggested and experimentally demonstrated subwavelength position localization of atoms using spatially varying energy shifts [6–8]. Zubairy and coworkers have discussed atom localization using resonance fluorescence and phase and amplitude control of the absorption spectrum [9–11]. Knight and colleagues discussed localization via quantum interference at the probability amplitude of the excited electronic state [12]. Li *et al.* have experimentally demonstrated probe narrowing beyond the diffraction limit by using a spatially varying coupling laser profile in a vapor cell [13]. Similar tools have been proposed for nanolithography using atomic beams [14]. There has also been remarkable progress in utilizing position-dependent stimulated emission to achieve nanoscale resolution [15,16]. This last approach, also known as *stimulated-emission depletion microscopy*, is now a widely used technique in biological imaging. We note that our approach of using the dark state for atomic localization has the following key advantages: (1) For the ideal case of sufficiently slowly varying driving laser pulses, the dark-state technique has no population at the excited electronic state. As a result, the atomic localization can, in principle, be achieved without suffering from the detrimental effects of spontaneous emission. This is especially important for quantum computing applications [2], where coherent manipulation with little decoherence is essential. (2) The dark state can be prepared adiabatically by using a counter-intuitive pulse sequence. As a result, as discussed in detail in Ref. [3], the scheme is insensitive to many experimental fluctuations, such as the intensity and timing jitter of the driving laser pulses. (3) Since the scheme is coherent, localization can be achieved at faster time scales at the expense of requiring more intense laser beams. Although in this work we use ∼100-ns-long laser pulses, dark-state-based localization can easily be achieved at subnanosecond time scales by using more powerful laser beams.

We next discuss the details of our experiment, which can be viewed as a proof-of-principle demonstration of the suggestion by Lukin and colleagues [2]. The experiment is performed inside a 14-port, stainless-steel ultrahigh vacuum chamber, which is kept at a base pressure of about 10^{-9} Torr. To construct the ^{87}Rb MOT, we use three counter-propagating beam pairs that are locked to the cycling transition, each with a beam power of 100 mW and a beam size of 3 cm. The MOT lasers are obtained from an external cavity diode laser whose output is amplified with a tapered amplifier. We typically trap about 1 billion ^{87}Rb atoms at a temperature of 150 μK. The EIT beams are derived from a separate master diode laser that is saturated-absorption locked to the appropriate transition. The coupling laser beam is shifted by 6.8 GHz using high-frequency acousto-optic modulators and is amplified with a tapered amplifier [17]. As shown in Fig. 1, the probe and the coupling lasers are resonant with $|F = 1\rangle \rightarrow |F' = 2\rangle$ and $|F = 2\rangle \rightarrow |F' = 2\rangle$ transitions of the D_2 line, near a wavelength of 780 nm. The beams have the same circular polarization, and the experiment works in three parallel m_F channels [18]. The coupling laser is split into two beams, which then reconverge at the MOT at an angle of 3 mrad to form a vertical standing wave with a spatial period of $\Lambda = 600\ \mu$m. We probe the localization by level-dependent fluorescence of the atomic cloud. The fluorescence signal is collected with a 2-in. achromatic doublet outside of the vacuum chamber and is recorded with an electron-multiplying CCD camera.

 ©2011 American Physical Society

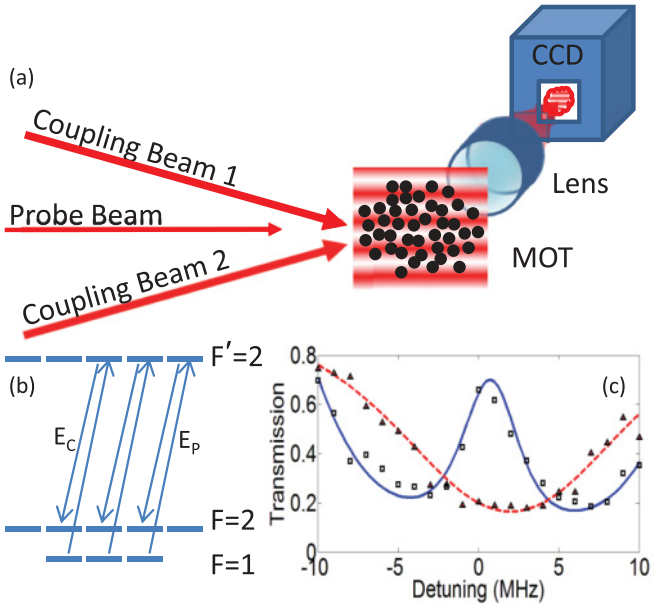

FIG. 1. (Color online) (a) The schematic of our experiment. The experiment is performed in a magneto-optical trap (MOT) of ultracold ^{87}Rb atoms. With atoms starting in the $|F = 1\rangle$ hyperfine level, we drive the atoms to the dark state with a probe laser beam and a spatially varying coupling laser beam. The spatial profile for the coupling laser is obtained by combining two identical beams at the MOT at an angle of 3 mrad, producing a vertical standing wave. The atomic localization is measured by taking fluorescence images with a CCD camera. (b) The relevant energy level diagram, with probe laser E_P and coupling laser E_C. The experiment works with three parallel m_F channels. (c) Transmission of a weak probe beam (∼100 nW power) through the cloud as a function of frequency with (squares) and without (triangles) the coupling laser beam. The lines are weak-probe electromagnetically induced transparency (EIT) line-shape (solid blue) and Lorentzian (dashed red) fits to the data. We perform this measurement with Coupling Beam 1 at an intensity of 120 mW/cm^2 and do not use the standing wave. The on-resonance transmission is about 70%, demonstrating reasonably good EIT.

Before proceeding further, we present a brief discussion of population localization using the dark state. Atoms distributed throughout the MOT will see different coupling laser intensities, based on where they are in the standing wave. Ignoring the complications due to parallel channels, the dark state of the atoms is given by [2–4]:

$$|\psi_{\text{dark}}(x)\rangle = \frac{\Omega_C(x)|F=1\rangle - \Omega_P|F=2\rangle}{\sqrt{\Omega_C(x)^2 + \Omega_P^2}}, \qquad (1)$$

where Ω_C and Ω_P are the Rabi frequencies of the respective beams. Here, for simplicity, we assume the probe beam to be uniform. The atoms can be prepared in the dark state of Eq. (1) by using the well-known counterintuitive pulse sequence with coupling laser turning on before the probe laser beam. Once the laser beams are turned on, they can be turned off simultaneously, preserving the ratio of the Rabi frequencies [3]. As a result, even after the laser pulses are turned off, the atomic system is left in the state determined by the probe and coupling laser Rabi frequencies at the temporal peak of the pulses. Through this preparation, atoms will

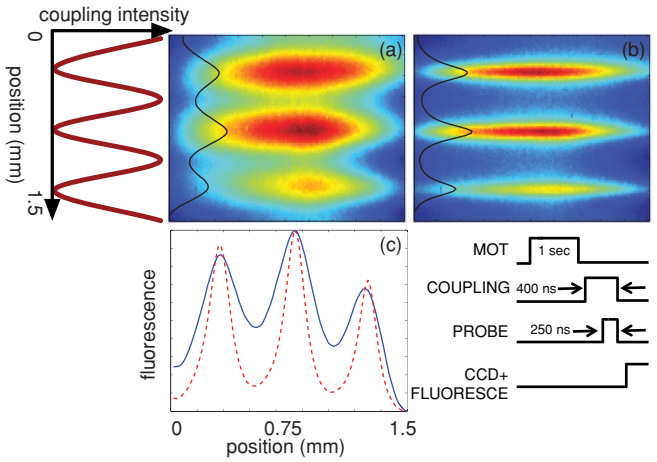

FIG. 2. (Color online) Fluorescence images of the atomic cloud for (a) $I_{C_0} \simeq 22 \times I_P$ and (b) $I_{C_0} \simeq 418 \times I_P$. The images are obtained by fluorescing the $|F = 2\rangle$ level via the cycling transition after the EIT beams are turned off. The fringes are confined to the intensity nodes of the coupling beam and become more localized as the intensity of the coupling laser increases. Panel (c) shows horizontally averaged line profiles of each fluorescence image for more direct comparison. The solid line is for the image in panel (a), and the dashed line is for the image in panel (b). The lower right diagram shows the experimental timing cycle.

populate $|F = 2\rangle$ with a probability of $|\langle F = 2|\psi_{\text{dark}}(x)\rangle|^2 = \Omega_P^2/[\Omega_C(x)^2 + \Omega_P^2]$. Due to the sensitive dependence of the dark state of EIT on the coupling beam intensity, atoms located near a coupling-field zero crossing (intensity node) coherently transfer to $|F = 2\rangle$ with high probability. If we assume that $\Omega_C(x)$ is linear near a zero crossing, then we expect the probability $|\langle F = 2|\psi_{\text{dark}}(x)\rangle|^2$ to be maximum at the coupling intensity node and have an approximate spatial width of $\sim\Lambda \cdot \Omega_P/\Omega_{C_0}$, where Ω_{C_0} is the peak coupling laser Rabi frequency [2,3]. As a result, with the probe laser intensity fixed, the population of level $|F = 2\rangle$ becomes more and more localized with increasing coupling-beam power.

The experimental timing cycle is shown in Fig. 2. We begin the experiment by loading the MOT for 1 s and then turn off the MOT magnetic field gradient 50 ms prior to the EIT beams to reduce Zeeman splitting of the magnetic sublevels. All atoms are then initialized to $|F = 1\rangle$ by turning off the hyperfine repumping laser for the MOT. We drive the atoms to the dark state by using a 400-ns-long coupling laser and a 250-ns-long probe laser beam. After the EIT beams are turned off, we probe the population of $|F = 2\rangle$ by fluorescing the atoms for 40 μs via the cycling transition ($|F = 2\rangle \rightarrow |F' = 3\rangle$). Due to sufficiently low atomic temperature, the motion of the atoms during fluorescence is negligible. In Fig. 2, we present two fluorescence images that show localization of the $|F = 2\rangle$ population as the coupling laser intensity is increased. Figure 2(a) illustrates a case in which we use a relatively weak coupling beam, where $I_{C_0} \simeq 22 \times I_P$ (I_{C_0} is the peak coupling intensity, and I_P is the probe intensity). The fringes align with the nodes of the coupling-beam intensity and have wide profiles in the vertical dimension. In Fig. 2(b), we use a coupling laser beam nearly 20 times more intense, such that $I_{C_0} \simeq 418 \times I_P$. We observe the fringes to be vertically

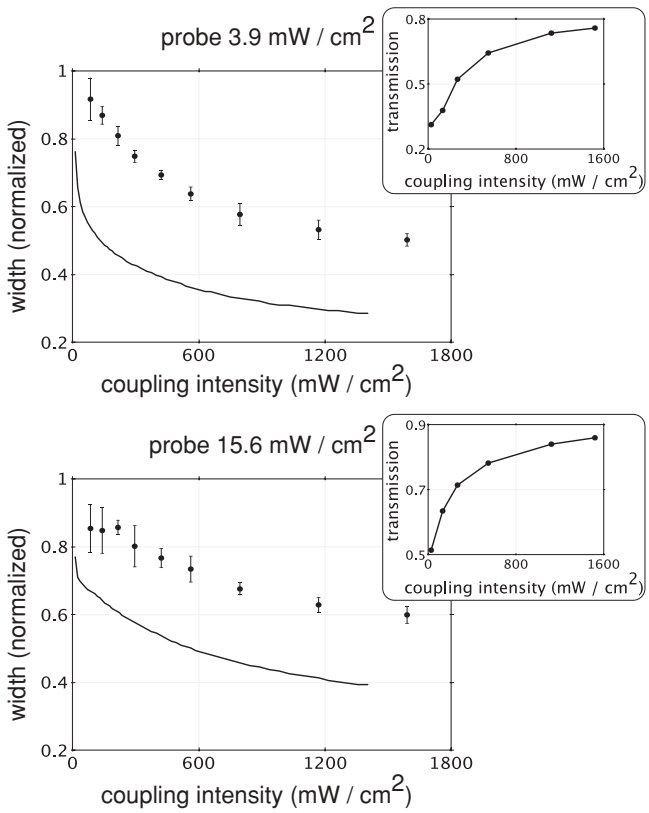

FIG. 3. The width of the fringes as a function of peak coupling-beam intensity for $I_P = 3.9$ mW/cm^2 and $I_P = 15.6$ mW/cm^2. The vertical scale is normalized such that one unit corresponds to a fringe width that equals half the spatial period (a sine wave). The population of $|F = 2\rangle$ becomes more tightly localized to the standing wave nodes with increasing coupling-laser beam intensity. The data points are experimental observations, and the solid lines are the results of numerical simulations. See the text for a discussion of the discrepancy between the experimental data and the numerical results. The insets show the integrated probe transmission through the cloud as the intensity of the coupling beam is increased. We observe increased transmission with increasing coupling-beam intensity, demonstrating the presence of EIT.

much more tightly confined to the coupling-beam nodes. Both pictures are based on a probe intensity of 3.9 mW/cm^2, and each picture is an average of 100 shots. Figure 2(c) shows horizontally averaged line profiles of each fluorescence image for a more direct comparison.

Figure 3 shows the normalized full-width-at-half-maximum (FWHM) of the fringes as the coupling-beam intensity is varied for two values of probe laser intensity, $I_P = 3.9$ mW/cm^2 and $I_P = 15.6$ mW/cm^2. Each data point is an average of 100 images, and the error bars show the standard deviation of each set. For $I_P = 3.9$ mW/cm^2, we observe the population of level $|F = 2\rangle$ to localize by about a factor of 2 as the coupling-beam intensity is increased. The solid lines in Fig. 3 are the results of numerical calculations without any adjustable parameters (i.e., each parameter that goes into the simulations is experimentally measured). Here, we include all relevant magnetic sublevels and numerically solve the time-domain density matrix equations for the conditions of our experiment. We have experimentally measured the standing-wave interference of the coupling laser beam to be slightly imperfect, with intensity contrast of 98%. This imperfection is included in our numerical calculations. At the moment, we do not completely understand the reason for the discrepancy between the numerical calculations and the experimental results. We have made measurements or estimates on various experimental imperfections, such as the interferometric fluctuations of the standing-wave intensity profile, the Zeeman shift of the magnetic sublevels due to a residual background magnetic field, and possible spatial misalignment of the beams from the center of the MOT. When these imperfections are included in the numerical calculations, we observe improved agreement between the theory and the experiment, although a large discrepancy still remains. Further investigations into the nature of the discrepancy are currently ongoing.

We next discuss the coherent nature of population localization. The insets in Fig. 3 show the integrated probe transmission through the atomic cloud as the coupling-beam intensity is increased. We see better probe transmission with increased coupling-beam intensity, demonstrating EIT for the exact conditions of each localization experiment. Furthermore, we have the ability to probe excited-state fluorescence during the EIT process by collecting scattered photons for the duration of the coupling laser beam. We observe a reduction in the excited-state fluorescence as the coupling-laser intensity is increased, complementing the probe transmission data of the insets in Fig. 3. We also observe a strong increase in the excited-state fluorescence when the coupling laser beam is turned off (probe laser propagating alone through the cloud) or when either laser is tuned away from resonance. This further

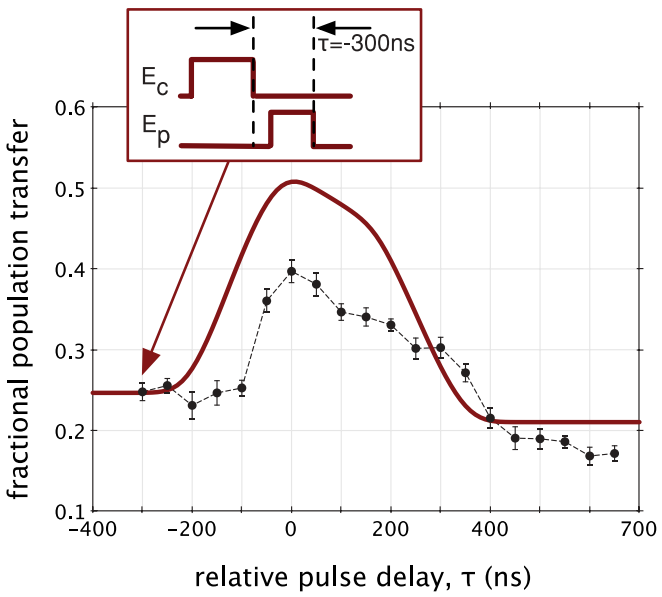

FIG. 4. (Color online) Demonstration of stimulated Raman adiabatic passage (STIRAP). For this test, we initialize the atoms to level $|F = 1\rangle$ and probe the population of $|F = 2\rangle$ as the overlap between the EIT pulses is varied. We observe maximal population transfer to $|F = 2\rangle$ when the coupling and probe pulses completely overlap. The solid line shows the result of a density matrix calculation with only one adjustable parameter.

confirms that the atoms are driven to a dark state, with a small population at the excited electronic level.

To further test the coherent nature of the population transfer, we have performed a stimulated Raman adiabatic passage (STIRAP) experiment [19]. We measure the population transfer to $|F = 2\rangle$ at the intensity peaks of the coupling laser using a pulse sequence similar to the one described above, but changing the relative temporal delay, τ, between the EIT beams. As shown in Fig. 4, we observe an increase in the population transfer to $|F = 2\rangle$ when the probe and coupling pulses overlap. For $\tau = -300$ ns, the coupling laser is turned off before the probe laser is turned on. For this case, there is no EIT, and the observed population transfer of 25% is due to optical pumping by the probe pulse. The solid line shows the result of a density matrix calculation in which the only adjustable parameter is the scaling of the probe- and coupling-laser intensities by the same factor, to account for possible misalignment of the beams from the MOT. This parameter is varied until the calculations match the observed population transfer at large negative delays. To increase contrast, the STIRAP experiments depicted in Fig. 4 use beams of 12 MHz detuned to the blue of the excited state. The predicted intensities of the two beams at the center of the MOT are $I_{C_0} \approx I_P = 16\ \mathrm{mW/cm^2}$.

To summarize, we have demonstrated localization of level population using EIT. As mentioned before, because our imaging system cannot resolve subwavelength spatial scales, we have performed this experiment with a small angle between the two coupling-laser beams, and therefore with a large spatial period of the standing-wave interference pattern. Future work will include extending this technique to the subwavelength regime and will possibly demonstrate nanometer-scale localization and addressing of neutral atoms. Furthermore, by using more powerful laser beams, we aim to explore atomic localization at much faster time scales. If we are successful, the ability to address atoms at subnanosecond time scales with subwavelength resolution may provide a powerful tool for solving many challenging problems, including the initialization and addressability of a neutral-atom quantum register [20,21].

We thank J. P. Sheehan for assistance with the experiment. This work was supported by the Air Force Office of Scientific Research (AFOSR).

[1] G. S. Agarwal and K. T. Kapale, J. Phys. B **39**, 3437 (2006).
[2] A. V. Gorshkov, L. Jiang, M. Greiner, P. Zoller, and M. D. Lukin, Phys. Rev. Lett. **100**, 093005 (2008).
[3] D. D. Yavuz and N. A. Proite, Phys. Rev. A **76**, 041802 (2007).
[4] S. E. Harris, Phys. Today **50**, 36 (1997).
[5] M. O. Scully and M. S. Zubairy, *Quantum Optics* (Cambridge University Press, Cambridge, UK, 1997).
[6] J. E. Thomas, Opt. Lett. **14**, 1186 (1989).
[7] K. D. Stokes, C. Schnurr, J. R. Gardner, M. Marable, G. R. Welch, and J. E. Thomas, Phys. Rev. Lett. **67**, 1997 (1991).
[8] J. R. Gardner, M. L. Marable, G. R. Welch, and J. E. Thomas, Phys. Rev. Lett. **70**, 3404 (1993).
[9] M. Kiffner, J. Evers, and M. S. Zubairy, Phys. Rev. Lett. **100**, 073602 (2008).
[10] M. Macovei, J. Evers, C. H. Keitel, and M. S. Zubairy, Phys. Rev. A **75**, 033801 (2007).
[11] K. T. Kapale and M. S. Zubairy, Phys. Rev. A **73**, 023813 (2006).
[12] E. Paspalakis and P. L. Knight, Phys. Rev. A **63**, 065802 (2001).
[13] H. Li, V. A. Sautenkov, M. M. Kash, A. V. Sokolov, G. R. Welch, Y. V. Rostovtsev, M. S. Zubairy, and M. O. Scully, Phys. Rev. A **78**, 013803 (2008).
[14] J. Mompart, V. Ahufinger, and G. Birkl, Phys. Rev. A **79**, 053638 (2009).
[15] S. W. Hell, Science **316**, 1153 (2007).
[16] P. C. Maurer *et al.*, Nat. Phys. **6**, 912 (2010).
[17] B. E. Unks, N. A. Proite, and D. D. Yavuz, Rev. Sci. Instrum. **78**, 083108 (2007).
[18] D. A. Braje, V. Balić, G. Y. Yin, and S. E. Harris, Phys. Rev. A **68**, 041801 (2003).
[19] K. Bergmann, H. Theuer, and B. W. Shore, Rev. Mod. Phys. **70**, 1003 (1998).
[20] E. Urban, T. A. Johnson, T. Henage, L. Isenhower, D. D. Yavuz, T. G. Walker, and M. Saffman, Nat. Phys. **5**, 110 (2009).
[21] A. Gaetan, Y. Miroshnychenko, T. Wilk, A. Chotia, M. Viteau, D. Comparat, P. Pillet, A. Browaeys, and P. Grangier, Nat. Phys. **5**, 115 (2009).